Near-threshold π^- photoproduction on the deuteron

B. Strandberg,[1] K. G. Fissum,[2,*] J. R. M. Annand,[1] W. J. Briscoe,[3] J. Brudvik,[4] F. Cividini,[5] L. Clark,[1] E. J. Downie,[3] K. England,[6] G. Feldman,[3] D. I. Glazier,[1] K. Hamilton,[1] K. Hansen,[4] L. Isaksson,[4] R. Al Jebali,[1] M. A. Kovash,[7] A. E. Kudryavtsev,[3,8] V. Lensky,[8,9] S. Lipschutz,[3,†] M. Lundin,[4] M. Meshkian,[2] D. G. Middleton,[5,10] L. S. Myers,[11] D. O'Donnell,[1] G. V. O'Rielly,[12] B. Oussena,[3] M. F. Preston,[2] B. Schröder,[2,4] B. Seitz,[1] I. I. Strakovsky,[3] M. Taragin,[3] and V. E. Tarasov[8]
(PIONS@MAX-lab Collaboration)

[1]*School of Physics and Astronomy, University of Glasgow, Glasgow G12 8QQ, Scotland, United Kingdom*
[2]*Department of Physics, Lund University, SE-221 00 Lund, Sweden*
[3]*Institute for Nuclear Studies, Department of Physics, The George Washington University, Washington, DC 20052, USA*
[4]*MAX IV Laboratory, Lund University, SE-221 00 Lund, Sweden*
[5]*Institut für Kernphysik, Johannes Gutenberg-Universität Mainz, D-55099 Mainz, Germany*
[6]*College of Engineering, University of Massachusetts Dartmouth, North Dartmouth, Massachusetts 02747, USA*
[7]*Department of Physics and Astronomy, University of Kentucky, Lexington, Kentucky 40506, USA*
[8]*National Research Centre "Kurchatov Institute", Institute for Theoretical and Experimental Physics (ITEP), Moscow 117218, Russia*
[9]*Institut für Kernphysik & Cluster of Excellence PRISMA, Johannes Gutenberg Universitat, Mainz D-55099, Germany*
[10]*Mount Allison University, Sackville, New Brunswick, Canada E4L 1E6*
[11]*Bluffton University, 1 University Drive, Bluffton, Ohio 45817, USA*
[12]*Department of Physics, University of Massachusetts Dartmouth, Dartmouth, Massachusetts 02747, USA*

(Received 10 December 2018; revised manuscript received 9 December 2019; accepted 19 February 2020; published 16 March 2020)

The first experimental investigation of the near-threshold cross section for incoherent π^- photoproduction on the deuteron $\gamma d \to \pi^- pp$ is presented. The experimental technique involved detection of the ≈131 MeV γ ray resulting from the radiative capture of photoproduced π^- in the target. The total cross section was measured using an unpolarized tagged-photon beam, a liquid-deuterium target, and three very large NaI(Tl) spectrometers. The data are compared to theoretical models that give insight into the elementary reaction $\gamma n \to \pi^- p$ and pion-nucleon and nucleon-nucleon final-state interactions.

DOI: 10.1103/PhysRevC.101.035207

I. INTRODUCTION

Incoherent pion photoproduction on the deuteron, $\gamma d \to \pi NN$, provides information on the elementary reaction on the nucleon $\gamma N \to \pi N$ and on pion-nucleon (πN) and nucleon-nucleon (NN) final-state interactions (FSI). The near-threshold cross section for the elementary reaction is sensitive to the E_{0+} amplitude, which has a long history of theoretical studies closely related to measurements of near-threshold pion photoproduction [1]. Partial-wave analysis (PWA) [2] of experimental data sets may be used to obtain values for this and other photoproduction amplitudes. These are vital inputs to low-energy descriptions of hadron physics based on dispersion relations [3] or chiral perturbation theory (χPT) [4]. The latter, which is also used for comparison with experimental data in this article, is an effective field theory of quantum chromodynamics (QCD), where hadrons, instead of quarks and gluons, act as relevant degrees of freedom. χPT emerges from the QCD Lagrangian in the chiral limit of vanishing up and down quark masses ($m_u, m_d \to 0$) and thus offers a way to investigate the fundamental symmetries and interactions of the strong force in an energy regime where QCD is nonperturbative.

Tagged-photon beams combined with improved detector technology have substantially increased the size of the global pion-production data set in recent decades. However, most measurements have focused on the π^0 channel [5–8], as the elementary amplitude for π^0 production vanishes in the chiral limit. Thus the π^0 data allow for direct probing of chiral symmetry breaking phenomena. The most recent of these experiments [8] provided high-precision differential cross section and beam asymmetry data that have enabled stringent testing of χPT. Threshold measurements of charged pion

*Corresponding author: kevin.fissum@nuclear.lu.se
†Present address: National Superconducting Cyclotron Laboratory, Michigan State University, Michigan 48824, USA.

photoproduction are scarce in comparison. While the threshold cross section for π^+ photoproduction was established in Ref. [9], none of the $E_\gamma < 200$ MeV π^- measurements [10–13] have probed the near-threshold region, with the lowest-energy data point at ≈158 MeV [13], more than 10 MeV above threshold. This article reports the pioneering measurement of the total cross section for π^- photoproduction on the deuteron in the energy range 147–160 MeV. The well-understood radiative capture (RC) reaction on the deuteron, $\pi^- d \to \gamma nn$ [14], with an endpoint photon-energy of 131.4 MeV, is exploited in a novel way for the yield determination of the photoproduced π^-.

II. EXPERIMENTAL SETUP

The experiment was performed at the Tagged-Photon Facility [15] of the MAX IV Laboratory [16] in Sweden. A tagged-photon beam with energies of 140–160 MeV, created via the bremsstrahlung-tagging technique [17,18], was incident on a thin cylindrical Kapton vessel that contained liquid deuterium (LD_2) with density $\rho_D = (0.163 \pm 0.001)$ g/cm^3. The Kapton vessel was a cylinder of 170 mm length and 68 mm diameter, aligned along the axis of the photon beam. The vessel walls were 120 μm thick. The tagged-photon energies E_γ were determined by momentum analysis of the post-bremsstrahlung electrons using a dipole magnet together with a 64-channel focal-plane (FP) hodoscope [19]. The tagged-photon energy resolution was ±0.3 MeV. Electron arrival times at the hodoscope were digitized with multihit time-to-digital converters (TDCs). The post-bremsstrahlung electron counting rate (typically 0.1–1 MHz per FP channel), necessary for the photon-flux determination, was measured by scalers, normalized to the counting time. Tagging efficiency, the fraction of bremsstrahlung photons which passed through the photon-beam collimation system en route to the target, was measured daily. The mean tagging efficiency was $(\approx 23 \pm 2^{\text{sys.}})\%$.

Three large NaI(Tl) spectrometers, named Boston University Sodium Iodide (BUNI) [20], Compton and Two Photon Spectrometer (CATS) [21] and Detector Of Iodine And Sodium (DIANA) [22], were placed at laboratory angles $\theta = 60^\circ$, 120°, and 150° to detect RC photons originating from the LD_2 target. The positioning of the detectors relative to the beam and the target is depicted in Fig. 1. Each spectrometer consisted of a cylindrical core crystal surrounded by an annulus of optically isolated crystal segments. The segments were in turn surrounded by plastic scintillators. Scintillation light was read out by photomultiplier tubes (PMTs) attached to the rear faces of the scintillators. Analog signals from the PMTs were recorded by charge-integrating analog-to-digital converters (ADCs).

Data were recorded on an event-by-event basis. The data-acquisition and data-analysis software were based on ROOT [23] and RooFit [24] frameworks. The data acquisition was triggered by an energy deposition greater than ≈50 MeV in any NaI(Tl), which initiated the readout of the ADCs and started the TDCs. The TDC stop signals came from the post-bremsstrahlung electrons striking the FP channels. The ADC information was used to reconstruct detected photon

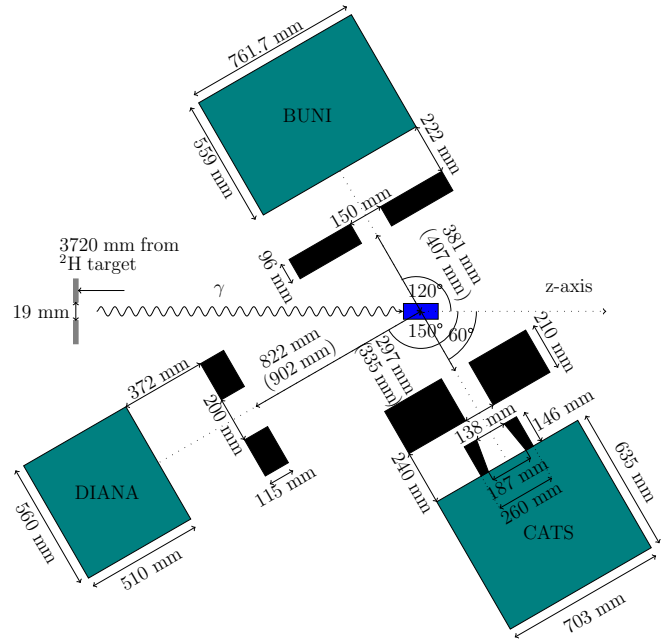

FIG. 1. A schematic plan view of the experimental setup. Gray: beam collimator; wavy line: photon beam; blue box: deuterium target; black regions: detector front and inner collimators; green boxes: scintillators (NaI(Tl) and plastics). The distances between the target and the detectors were different in 2011 and 2015. The 2011 values are indicated in brackets.

energies, whereas the FP TDC information established the coincidence between the post-bremsstrahlung recoil electrons and the particles detected with the spectrometers. The data were collected over three run periods in 2011 and 2015.

III. ANALYSIS

A. Calibration

Each NaI(Tl) detector was calibrated from its in-beam response to a low-intensity tagged-photon beam. Cosmic-ray muons that traversed the detectors during data taking were identified with the annulus scintillators by requiring coincident signals in opposing annular segments. Selection of the cosmic-ray events is illustrated in Fig. 2. Shifts in the pulse-height distributions of selected cosmic-ray muon events were used to correct for PMT gain instabilities. After calibration, the NaI(Tl) detectors had a resolution of ≈2% (full width at half maximum) for the incident photon energies. The absolute calibration of the tagged-photon energies and the NaI(Tl) detectors was determined with an accuracy of ±0.4 MeV by reconstructing the 131.4 MeV photon-energy endpoint from the RC reaction $\pi^- d \to \gamma nn$ [14].

B. Signal identification

Photons from the RC reaction were also used to determine the yield of photoproduced π^-. The near-threshold π^- had low kinetic energies and most were instantaneously captured inside the LD_2 target. The two dominant capture channels are nonradiative capture (NRC) $\pi^- d \to nn$

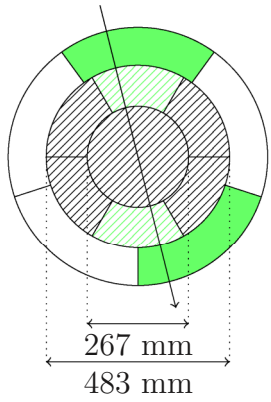

FIG. 2. Cross-sectional view of the CATS detector. Cosmic-ray muon events (downgoing arrow) that caused a signal in opposing annulus segments (green) were selected for monitoring PMT gain instabilities. NaI(Tl) crystals are striped to distinguish them from plastic scintillators [25].

(absolute branching ratio $\mathrm{BR_{nrc}} = 0.739 \pm 0.010$) and RC ($\mathrm{BR_{rc}} = 0.261 \pm 0.004$) [26]. Using these branching ratios and the energy spectrum of the RC photons [14,27,28], the π^- photoproduction yield was obtained. Figure 3 depicts the simulated energy spectra of the dominant background reactions of deuteron photodisintegration (*np sim*), π^0 photoproduction (π^0 *sim*), and π^- NRC (*nn sim*), alongside the theoretical RC spectrum (γnn *th*) [27,29], the simulated RC spectrum (γnn *sim*), and the measured energy spectrum (*exp. data*). Simulations were based on GEANT4 [30]. The photoproduced π^+ did not constitute a significant background, as the muons from the dominant subsequent decay $\pi^+ \to \mu^+\nu_\mu$ did not deposit more than ≈50 MeV in any of the NaI(Tl) detectors. Positrons from the decay $\mu^+ \to e^+\nu_e\bar{\nu}_\mu$ were almost always outside the timing coincidence window with respect to the post-bremsstrahlung electron. The simulated RC spectrum

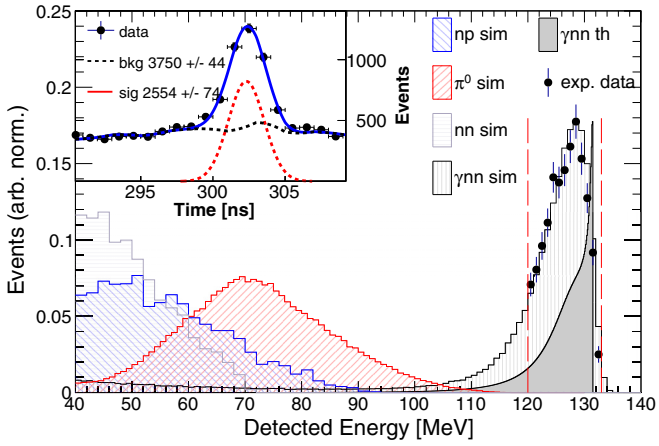

FIG. 3. Simulated energy spectra of dominant reaction channels alongside the measured energy spectrum and a theoretical energy spectrum of π^- RC. Inset: A typical fit to a timing-coincidence spectrum for events inside the cut $E_{\mathrm{det}} \in [120, 133]$ MeV for yield determination.

was obtained by first matching the Monte Carlo in-beam data to the experimental in-beam data [25,31]. Then, photons with energies sampled from the theoretical RC spectrum and an isotropic angular distribution were generated in the LD_2 target into 4π solid angle. Energy deposited by the photons in the NaI(Tl) detectors was smeared to account for the previously determined resolution effects, which led to the simulated RC spectrum (Fig. 3). The simulation, which is in excellent agreement with the data, indicated that the dominant background reactions could be removed by selecting the detected energy $E_{\mathrm{det}} \in [120, 133]$ MeV. Background from elastic $\gamma d \to \gamma d$ and inelastic $\gamma d \to \gamma np$ Compton scattering could not be separated. Contamination from Compton scattering channels was angle and energy dependent, but at the present energies the scattering cross section is only a few percent of the charged-pion photoproduction cross section. The cross-section data from Refs. [25,32] were extrapolated to produce conservative scattering-contamination estimates. These indicated that the effect on the extracted π^- cross section was typically ±3% (maximum of 5.5% at lowest E_γ). This effect was accounted for in the systematic uncertainty analysis discussed below.

C. Yield determination

The total cross section for π^- photoproduction on the deuteron was determined according to

$$\sigma = \frac{4\pi Y}{\Omega_{\mathrm{eff}} N_\gamma \kappa_{\mathrm{eff}} P_{\mathrm{c}}\, \mathrm{BR_{rc}}}, \tag{1}$$

where Y is the yield of RC photons, Ω_{eff} is the detector acceptance, N_γ is the tagged-photon flux incident on the target, κ_{eff} is the effective target thickness, P_{c} is the π^- capture probability inside the LD_2 target, and $\mathrm{BR_{rc}}$ is the branching ratio for RC. The factor 4π originates from the assumption that RC photons are emitted isotropically. For the yield determination, timing-coincidence spectra with respect to the post-bremsstrahlung recoil electrons were filled for events inside the cut $E_{\mathrm{det}} \in [120, 133]$ MeV. The FP channels were grouped in eight ≈2.5 MeV wide bins, resulting in eight spectra per detector. The resulting spectra had a coincidence peak superimposed upon events that were in random coincidence. As the dominant background reactions were removed by the cut on E_{det}, π^- capture yields could be determined directly from fits to the coincidence spectra (Fig. 3 inset). The signal peak was represented by a Gaussian. The background from random coincidences had a time structure due to a time modulation of the electron-beam intensity related to the pulse-stretching and beam-extraction apparatus [33]. The first two FP energy bins were below π^-/π^+ threshold. Thus, the coincidence spectra for these bins were completely dominated by random coincidences, which allowed estimation of the random-background shape. The background shape visible in the inset of Fig. 3 (black line) was obtained from the sub-pion-threshold data and employed in the fit of the super-pion-threshold data. Tools in the RooFit package enable creation of a fit shape from any histogram, which circumvents the difficulty of defining an analytical form for the nontrivial shape of the random background coincidences. The fit was moderately dependent

on the width of the fitted window around the coincidence peak, which led to a systematic uncertainty of ≈2% (7% at lowest E_γ). Systematic uncertainty due to contamination from π^- produced in the thin-walled Kapton vessel was estimated to be ≈1.5% by taking into account the chemical composition of Kapton, the thickness of the endcaps of the vessel, and assuming conservatively that the π^- photoproduction cross section on ^{12}C and ^{16}O scales linearly with the number of neutrons per atom.

D. Detector acceptances

The detector acceptance Ω_{eff} was determined from the simulated RC spectrum described previously. The detector acceptance was determined by

$$\Omega_{\text{eff}} = 4\pi N_{E_{\text{det}}\in[120,133]\ \text{MeV}}/N_{\text{tot}}, \tag{2}$$

where N_{tot} is the total number of Monte Carlo photons simulated inside the target, with energies sampled from the theoretical RC spectrum and directions sampled from a phase-space distribution over 4π solid angle. The numerator is the number of events in a detector within the energy cut $E_{\text{det}} \in [120, 133]$ MeV. The acceptances of the detectors at 60°, 120°, and 150° were ≈46 msr, ≈30 msr, and ≈26 msr, respectively. The dominant systematic uncertainty of 5% originated from the uncertainty in the theoretical model for RC [29]. Systematic uncertainty from the positioning accuracy of the detectors and the target was estimated to be ≈3% by varying the detector and target positions in the simulation within realistic limits. The ±0.4 MeV uncertainty in the overall energy calibration of the detectors propagated into the acceptance calculation and was estimated to have an effect of ≈1.5% by varying the energy cut by the uncertainty in the simulation and recording the effect on the acceptance.

E. Tagged-photon flux and target thickness

The tagged-photon flux N_γ was established by multiplying the FP hodoscope counts by the measured tagging efficiencies (≈2% systematic uncertainty from tagging efficiency). The effective target thickness was

$$\kappa_{\text{eff}} = (8.14 \pm 0.10) \times 10^{23}\ \text{nuclei/cm}^2, \tag{3}$$

with a ≈1.2% systematic uncertainty originating from the geometry of the target. Further details about N_γ and κ_{eff} can be found in Ref. [25].

F. Pion-capture probability

The capture probability of photoproduced π^- P_c was estimated from a GEANT4 simulation, where π^- were simulated inside the LD_2 target. The X-Y coordinates of the vertices were sampled from a simulated intensity distribution of the photon beam determined by the geometry of the beam line, and the Z coordinates (along the beam axis) were distributed uniformly over the length of the target. In sampling the momenta of the π^-, the Fermi momentum of the bound neutron in the deuteron [34], the energy of the incident photon, and the angular distribution of the pions in the elementary photoproduction reaction [35] were taken into account. The dominant systematic uncertainty of $\lesssim$3.1% originated from the ±0.4 MeV uncertainty in the tagged-photon energies. The effect of uncertainty in the beam profile was estimated to be $\lesssim$1.6% by changing the beam radius by ±10% in the simulation and recording the effect on P_c. The simulated radius of the photon beam spot at the target center, $r_{\text{beam}} \approx 20$ mm, was in good agreement with a beam photograph at that location and was substantially smaller than the $r_{\text{vessel}} = 34$ mm radius of the Kapton vessel. Additionally, the π^- escape from the target occurred predominantly from the downstream endcap, which explains the relatively weak dependence on the radius of the beam. Figure 4 depicts the dependence of P_c on the incident photon energy E_γ with systematic uncertainties.

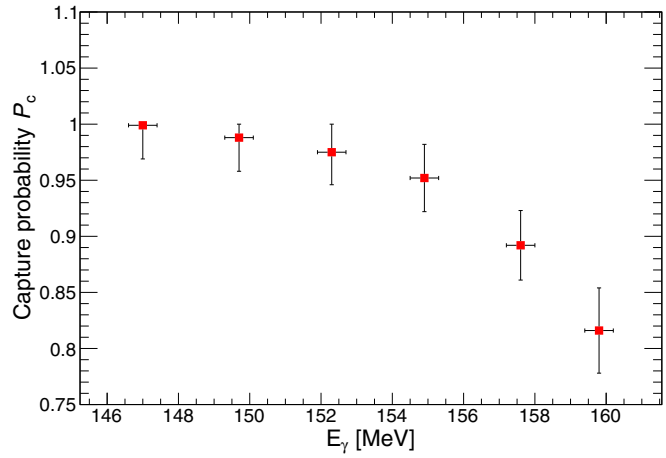

FIG. 4. Probability of π^- capture inside the LD_2 target with systematic uncertainties as a function of the incident photon energy E_γ.

G. Results

The cross section for threshold π^- photoproduction at each energy was determined as a statistically weighted average of nine measurements (three detectors and three run periods). The standard deviation of the nine measurements was used to estimate the combined systematic uncertainty. Sources of systematic uncertainties are summarized in Table I. The right

TABLE I. Summary of the dominant systematic uncertainties. The right column indicates if the systematic uncertainty contributes to the standard deviation of the nine cross-section measurements.

Quantity	Source	Magnitude	In std. dev.
Y	fit	2%–7%	✓
	scattering	$\lesssim$5.5%	✓
	Kapton	1.5%	
Ω_{eff}	positioning	3%	✓
	E_{cut}	1.5%	✓
	model	5%	
N_γ	tagg. eff.	2%	✓
κ_{eff}	geometry	1.2%	
P_c	beam sim.	$\lesssim$1.6%	
	ΔE_γ	$\lesssim$3.1%	
BR_{rc}	measurement	1.5%	

TABLE II. Measured total cross section for π^- photoproduction on the deuteron with statistical and systematic uncertainties.

E_γ (MeV)	$\sigma \pm \text{err}_{\text{stat.}} \pm \text{err}_{\text{sys.}}$ (μb)
147.0	3.8 ± 0.2 (5.3%) ± 1.1 (28.9%)
149.7	11.9 ± 0.3 (2.5%) ± 1.8 (15.1%)
152.3	21.4 ± 0.3 (1.4%) ± 2.5 (11.7%)
154.9	28.5 ± 0.5 (1.8%) ± 3.0 (10.5%)
157.6	31.9 ± 0.4 (1.3%) ± 3.0 (9.4%)
159.8	35.0 ± 0.5 (1.4%) ± 3.4 (9.7%)

column of Table I specifies whether or not a given systematic uncertainty contributed to the standard deviation of the nine measurements. Typically, the uncertainty estimated from the standard deviation was of similar magnitude compared to the uncertainty estimated from adding the contributing sources in quadrature. The noncontributing sources were then added to the standard deviation in quadrature to produce the final systematic uncertainties (Table II, Fig. 5). Of the noncontributing uncertainties, only the capture efficiency affected the shape of the cross-section curve. Others affected the scale of the results. The angle- and energy-dependent uncertainties from scattering channels are accounted for in the standard deviation of the combined result, as they contributed to the observed spread of the nine measurements. A full account of the analysis of the experimental data is available in Ref. [36].

IV. THEORETICAL ANALYSIS

The experimental data for the $\gamma d \to \pi^- pp$ reaction are now compared with model predictions. Compared to the elementary reaction $\gamma n \to \pi^- p$, the additional final-state proton introduces additional FSI that have a non-negligible effect on the cross section. The model is a version of that described in Ref. [38], simplified for the near-threshold region. It is

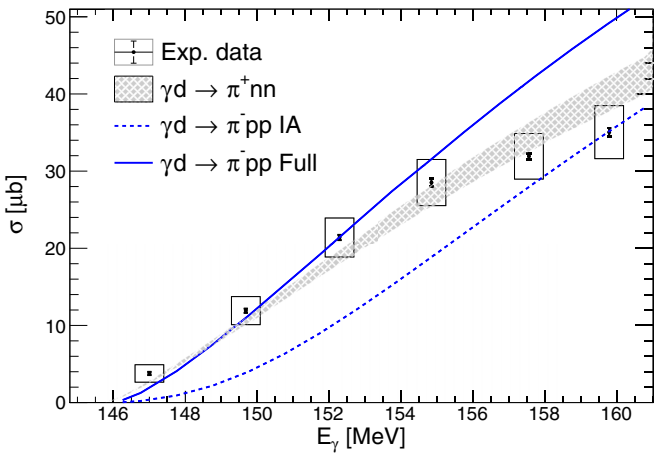

FIG. 5. Measured total cross section for π^- photoproduction on the deuteron with statistical (error bars) and systematic (error boxes) uncertainties alongside theoretical predictions for $\gamma d \to \pi^+ nn$ (gray band) [37] and $\gamma d \to \pi^- pp$ in the impulse approximation (blue dashed line) and with FSI (blue solid line) [38].

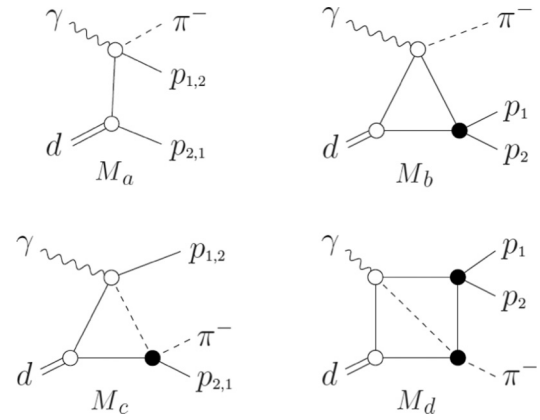

FIG. 6. IA (M_a), NN-FSI (M_b), πN-FSI (M_c) and two-loop (M_d) diagram for $\gamma d \to \pi^- pp$. Filled black circles indicate FSI vertices.

calculated from the four diagrams displayed in Fig. 6, where M_a is the impulse approximation (IA) term, M_b and M_c are the NN and πN FSI terms, and M_d is the NN-FSI term with pion rescattering in the intermediate state (the "two-loop" term). The ingredients and the approximations for the computation of the four terms are given in the following list.

(1) The elementary reaction is described by the s-wave amplitude, which is determined by the E_{0+} multipole. The value of E_{0+} as extracted by various analyses has been very stable over the last decades and here $E_{0+} = -31.9$ from Ref. [1] is used. Here and elsewhere in the article the E_{0+} amplitude is expressed in the conventional units of $10^{-3}/m_{\pi^+}$. Further, in diagrams M_c and M_d of Fig. 6, only charged intermediate pions are included as the neutral-pion photoproduction amplitude is much smaller than the charged-pion photoproduction amplitude in the near-threshold region. In this approximation, the cross section is proportional to $|E_{0+}|^2$.

(2) The s-wave pp-scattering amplitude includes Coulomb effects and is taken in the effective-range approximation [39], using the values $a_{pp} = -7.8$ fm for the pp scattering length and $r_{pp} = 2.8$ fm for the effective range. Off-shell effects are included as in Refs. [38,40].

(3) For πN scattering, the s-wave πN amplitude $f_{\pi^- p} = b_0 - b_1$ is used, fixed by the isospin scattering lengths $b_0 = -28$ and $b_1 = -881$ in units of $10^{-4}/m_\pi$ [41].

(4) The deuteron wave function (DWF) derived from the Bonn potential is used in the parameterized form from Ref. [42]. The IA diagram M_a includes both the s- and d-wave parts of the DWF, with the d wave having only a small effect on the cross section at energies close to threshold. The inclusion of the d wave in other diagrams is expected to have a negligible effect and is neglected to simplify calculations.

The cross-section model is compared with the experimental data in Fig. 5. The dashed curve indicates the IA (M_a in Fig. 6), whereas the solid curve indicates the full model

(all terms in Fig. 6). The dominant correction to the IA term M_a originates from the NN-FSI amplitude M_b, whereas the combined contribution from the πN-FSI (M_c) and the two-loop term (M_d) is typically $\lesssim$10%. Considering terms M_c and M_d, the relative contribution of M_c to the combined result of M_a and M_b is stable at around $\approx$4%, while the effect of M_d reduces from $\approx$8% to $\approx$2% as E_γ increases from threshold to $\approx$160 MeV. While the model and the experimental data agree within uncertainties in the energy region 147–157 MeV, it overestimates the data above 157 MeV, due to two dominant factors:

(1) The model does not account for the energy dependence of E_{0+}. Since E_{0+} decreases with energy, this causes the theoretical model to overestimate the cross section as E_γ increases from threshold.
(2) The model uses only the s-wave amplitude for the elementary reaction $\gamma n \to \pi^- p$ and for NN-FSI, which is expected to contribute to the divergence as higher partial waves become significant at energies $\gtrsim$10 MeV above threshold.

The measured cross section for $\gamma d \to \pi^- pp$ is also compared to a previous χPT prediction for the isospin-partner channel $\gamma d \to \pi^+ nn$ [37]. Comparison of the π^- experimental data with the π^+ prediction is insightful as, compared to Ref. [38], the χPT calculation uses higher-order partial waves both for the elementary reaction $\gamma p \to \pi^+ n$ and for the NN-FSI. It also accounts for the energy dependence of E_{0+}. In the leading order of the chiral expansion, the elementary amplitudes $\gamma n \to \pi^- p$ and $\gamma p \to \pi^+ n$ are equal. The most important difference between the elementary π^+ and π^- photoproduction reactions is the proton recoil in the latter, which increases the dipole moment of the final πN system. Due to the absence of proton recoil in the π^+ reaction, the absolute value of E_{0+} is approximately 12% smaller for $\gamma p \to \pi^+ n$ compared to $\gamma n \to \pi^- p$. For this calculation $E_{0+}(\pi^+ n) = 28.2$ from Ref. [43] was used. This effect suppresses the cross section for $\gamma d \to \pi^+ nn$ compared to $\gamma d \to \pi^- pp$. On the other hand, there is no Coulomb FSI in $\gamma d \to \pi^+ nn$, which leads to a relative increase in the cross section compared to $\gamma d \to \pi^- pp$. These two effects are expected to cancel partially. The χPT calculation for $\gamma d \to \pi^+ nn$ with theoretical uncertainties (see Ref. [37] for details of the uncertainty calculation) is depicted as a gray band in Fig. 5. The starting E_γ value of the theoretical curve has been shifted to 145.8 MeV to account for the difference in the reaction threshold compared to the π^- channel. The calculation has been performed at the order $\chi^{5/2}$ of the chiral expansion parameter $\chi = m_\pi/m_N$, where m_π (m_N) stands for the generic pion (nucleon) mass. The experimental data and the $\gamma d \to \pi^+ nn$ model agree within uncertainties, suggesting that the differences between the π^+ and π^- channels indeed tend largely to cancel. The good agreement between the models and the experimental data at energies $E_\gamma < 157$ MeV suggests that in the immediate vicinity of the threshold, the dominant processes that contribute to the cross section are relatively well understood.

V. SUMMARY

In summary, the first measurement of the near-threshold cross section for π^- photoproduction on the deuteron has been presented along with model predictions. The models and the experimental data are in good agreement in the vicinity of the threshold and provide new insight into the FSI behavior in this energy regime. The behavior further away from the threshold could be investigated by a dedicated χPT calculation for the measured $\gamma d \to \pi^- pp$ reaction. Further insight into the discrepancies between experimental data and the models at energies $\gtrsim$10 MeV above threshold could be gained from differential cross-section measurements for $\gamma d \to \pi^- pp$, which would allow for a more detailed study of the effects of various partial waves.

ACKNOWLEDGMENTS

The authors would like to thank W. R. Gibbs, B. F. Gibson, and G. F. de Téramond for constructive discussions. The authors acknowledge support from the staff of the MAX IV Laboratory. This research has been supported by the Swedish Research Council (Contracts No. 40324901 and No. 80410001), the Crafoord Foundation (Grant No. 20060749), the Scottish Universities Physics Alliance (SUPA), the SUPA Prize Studentship, UK STFC Grants No. 57071/1 and No. 50727/1, U.S. NSF Grant No. PHY1309130, U.S. DOE Grants No. DE–SC0016581, No. DE–SC0016583 and No. DE–FG02–06ER41422, the NFS/IRES Award No. 0553467, RFBR Grants No. 16–02–00767 and No. 16–02–00767a, and the Deutsche Forschungsgemeinschaft (DFG) through the Collaborative Research Center, SFB 1044.

[1] D. Drechsel and L. Tiator, J. Phys. G **18**, 449 (1992), and references therein.
[2] R. A. Arndt, R. L. Workman, Z. Li, and L. D. Roper, Phys. Rev. C **42**, 1853 (1990).
[3] D. Drechsel, B. Pasquini, and L. Tiator, Few-Body Syst. **41**, 13 (2007).
[4] M. Hilt, B. C. Lehnhart, S. Scherer, and L. Tiator, Phys. Rev. C **88**, 055207 (2013), and references therein.
[5] J. C. Bergstrom, J. M. Vogt, R. Igarashi, K. J. Keeter, E. L. Hallin, G. A. Retzlaff, D. M. Skopik, and E. C. Booth, Phys. Rev. C **53**, R1052(R) (1996).
[6] J. C. Bergstrom, R. Igarashi, and J. M. Vogt, Phys. Rev. C **55**, 2016 (1997).
[7] J. C. Bergstrom, Phys. Rev. C **58**, 2574 (1998).
[8] D. Hornidge, P. Aguar Bartolomé, J. R. M. Annand, H. J. Arends, R. Beck, V. Bekrenev, H. Berghäuser, A. M. Bernstein, A. Braghieri, W. J. Briscoe *et al.* (A2 Collaboration and CB-TAPS Collaboration), Phys. Rev. Lett. **111**, 062004 (2013).
[9] E. C. Booth, B. Chasan, J. Comuzzi, and P. Bosted, Phys. Rev. C **20**, 1217 (1979).
[10] V. Rossi, A. Piazza, G. Susinno, F. Carbonara, G. Gialanella, M. Napolitano, R. Rinzivillo, L. Votano, G. C.

Mantovani, A. Piazzoli *et al.*, Nuovo Cimento A **13**, 59 (1973).
[11] M. Salomon, D. Measday, J.-M. Poutissou, and B. Robertson, Nucl. Phys. A **414**, 493 (1984).
[12] M. Wang, Ph.D. thesis, University of Kentucky, 1992 (unpublished).
[13] K. Liu, Ph.D. thesis, University of Kentucky, 1994 (unpublished).
[14] B. Gabioud, J.-C. Alder, C. Joseph, J.-F. Loude, N. Morel, A. Perrenoud, J.-P. Perroud, M. T. Tran, E. Winkelmann, W. Dahme *et al.*, Phys. Rev. Lett. **42**, 1508 (1979).
[15] J.-O. Adler, M. Boland, J. Brudvik, K. Fissum, K. Hansen, L. Isaksson, P. Lilja, L.-J. Lindgren, M. Lundin, B. Nilsson *et al.*, Nucl. Instrum. Methods Phys. Res. Sect. A **715**, 1 (2013).
[16] M. Eriksson, in *Proceedings of the 5th International Particle Accelerator Conference, IPAC, Dresden, Germany* (Joint Accelerator Conferences Website, JACoW, Geneva, Switzerland, 2014), pp. 2852–2855.
[17] J.-O. Adler, B.-E. Andersson, K. I. Blomqvist, B. Forkman, K. Hansen, L. Isaksson, K. Lindgren, D. Nilsson, A. Sandell, B. Schröder *et al.*, Nucl. Instrum. Methods Phys. Res. Sect. A **294**, 15 (1990).
[18] J.-O. Adler, B.-E. Andersson, K. I. Blomqvist, K. G. Fissum, K. Hansen, L. Isaksson, B. Nilsson, D. Nilsson, H. Ruijter, A. Sandell *et al.*, Nucl. Instrum. Methods Phys. Res. Sect. A **388**, 17 (1997).
[19] J. M. Vogt, R. E. Pywell, D. M. Skopik, E. L. Hallin, J. C. Bergstrom, H. S. Caplan, K. I. Blomqvist, W. D. Bianco, and J. W. Jury, Nucl. Instrum. Methods Phys. Res. Sect. A **324**, 198 (1993).
[20] J. P. Miller, E. J. Austin, E. C. Booth, K. P. Gall, E. K. McIntyre, and D. A. Whitehouse, Nucl. Instrum. Methods Phys. Res. Sect. A **270**, 431 (1988).
[21] A. Hünger, J. Peise, A. Robbiano, J. Ahrens, I. Anthony, H.-J. Arends, R. Beck, G. Capitani, B. Dolbilkin, H. Falkenberg *et al.*, Nucl. Phys. A **620**, 385 (1997).
[22] L. S. Myers, Ph.D. thesis, University of Illinois at Urbana-Champaign, 2010, http://hdl.handle.net/2142/18332.
[23] R. Brun and F. Rademakers, Nucl. Instrum. Methods Phys. Res. A **389**, 81 (1997).
[24] W. Verkerke and D. Kirkby, arXiv:physics/0306116 (2003).
[25] B. Strandberg, J. R. M. Annand, W. Briscoe, J. Brudvik, F. Cividini, L. Clark, E. J. Downie, K. England, G. Feldman, K. G. Fissum, D. I. Glazier, K. Hamilton, K. Hansen, L. Isaksson, R. A. Jebali, M. A. Kovash, S. Lipschutz, M. Lundin, M. Meshkian, D. G. Middleton, L. S. Myers, D. O'Donnell, G. O'Rielly, B. Oussena, M. F. Preston, B. Schroder, B. Seitz, I. Strakovsky, and M. Taragin (The COMPTON@MAX-lab Collaboration), Phys. Rev. C **98**, 012201(R) (2018).
[26] V. L. Highland, M. Salomon, M. Hasinoff, E. Mazzucato, D. Measday, J.-M. Poutissou, and T. Suzuki, Nucl. Phys. A **365**, 333 (1981).
[27] W. R. Gibbs, B. F. Gibson, and G. J. Stephenson, Jr., Phys. Rev. C **11**, 90 (1975).
[28] G. F. de Téramond, Phys. Rev. C **16**, 1976 (1977).
[29] W. R. Gibbs and B. F. Gibson (private communication).
[30] J. Allison, K. Amako, J. Apostolakis, P. Arce, M. Asai, T. Aso, E. Bagli, A. Bagulya, S. Banerjee, G. Barrand *et al.*, Nucl. Instrum. Methods Phys. Res. A **835**, 186 (2016).
[31] L. S. Myers, J. R. M. Annand, J. Brudvik, G. Feldman, K. G. Fissum, H. W. Grießhammer, K. Hansen, S. S. Henshaw, L. Isaksson, R. Jebali *et al.*, Phys. Rev. C **92**, 025203 (2015).
[32] K. Kossert, M. Camen, F. Wissmann, J. Ahrens, J. R. M. Annand, H.-J. Arends, R. Beck, G. Caselotti, P. Grabmayr, O. Jahn *et al.*, Phys. Rev. Lett. **88**, 162301 (2002).
[33] R. Al Jebali, Ph.D. thesis, The University Of Glasgow, Scotland, 2013, http://theses.gla.ac.uk/4467/1/2013aljebaliphd.pdf.
[34] M. Lacombe, B. Loiseau, R. Mau, J. Côté, P. Pirés, and R. de Tourreil, Phys. Lett. B **101**, 139 (1981).
[35] W. J. Briscoe, I. I. Strakovsky, and R. L. Workman, Institute of Nuclear Studies of The George Washington University Database [SAID], http://gwdac.phys.gwu.edu.
[36] B. Strandberg, Ph.D. thesis, University Of Glasgow, 2017, http://theses.gla.ac.uk/8362/7/2017StrandbergPhD.pdf.
[37] V. Lensky, V. Baru, J. Haidenbauer, C. Hanhart, A. Kudryavtsev, and U. G. Meißner, Eur. Phys. J. A **26**, 107 (2005).
[38] V. E. Tarasov, W. J. Briscoe, H. Gao, A. E. Kudryavtsev, and I. I. Strakovsky, Phys. Rev. C **84**, 035203 (2011).
[39] L. D. Landau and E. M. Lifshits, *Quantum Mechanics: Non-Relativistic Theory* (Pergamon, Oxford, 1965).
[40] M. I. Levchuk, A. Y. Loginov, A. A. Sidorov, V. N. Stibunov, and M. Schumacher, Phys. Rev. C **74**, 014004 (2006).
[41] M. Döring, E. Oset, and M. J. V. Vacas, Phys. Rev. C **70**, 045203 (2004).
[42] R. Machleidt, Phys. Rev. C **63**, 024001 (2001).
[43] V. Bernard, N. Kaiser, and U.-G. Meißner, Phys. Lett. B **383**, 116 (1996).